Electronic Supplementary Material (ESI) for Journal of Materials Chemistry A.
This journal is © The Royal Society of Chemistry 2019

Electronic Supplementary Information

Abnormal thermal stability of sub-10 nm Au nanoparticles and their high catalytic activity

Xiaoqing Cao,‡ Jun Zhou,‡ Hongna Wang, Song Li,* Wei Wang, Gaowu Qin*

Key Laboratory for Anisotropy and Texture of Materials，School of Materials Science and Engineering，Northeastern University，Shenyang 110819, China

*Email: lis@atm.neu.edu.cn, qingw@smm.neu.edu.cn.

‡Xiaoqing Cao and Jun Zhou contributed equally to this work.

The experimental process of plasma electrolytic oxidation (PEO)

(1) The MgO film was deposited by the application of a 100v voltage on Mg plate 10min in basic electrolyte (4 g L^{-1} $Na_2SiO_3 \cdot 9H_2O$, 12 g L^{-1} KOH and 8 g L^{-1} NaF in 500 mL water); this process is a conventional anodic oxidation process and the mainly purpose is to fabricate MgO as a barrier layer which is advantageous to arc discharge-starting and arc-stabling in following working mode;

(2) The $HAuCl_4$ is dissolved in basic electrolyte and the Mg plate (with MgO film) is treated by PEO in a working mode (current i=0.4 A, frequency f=500 Hz, duty cycle d=35%, time t=3 min, electrolyte temperature T=15 °C); In this process, the applied current flowing would easily increase the prefabricated MgO film thickness, which could be regarded as a resistor and correspondingly cause an improvement in voltage. Next, the dielectric breakdown would occur in relatively thin region of film due to the less resistance and therefore the arc-discharging emerges, which lead to a breakdown for the prepared MgO film breakdown and disappear quickly. This phenomenon (arc-charging) is also explained by Ikonopisov (Electrochim Acta 1977;22: 1077–1782) due to the plasma generation because of electron avalanche theory.

After arc discharge-starting, the original MgO film disappears and would produce a new porous MgO film. The arc discharge cause the local high temperature and high pressure that trigger a plasma chemical reaction in these arcing sites. In this process, the surface metal Mg is gasified and oxidized to form MgO and $[AuCl_4]^-$ ion in electrolyte (attracted by anode Mg) is high temperature decomposed to form Au species. Once the arc discharge disappears, the MgO and Au species are simultaneously quenched by the cooling electrolyte and turn into a coating layer on Mg plate. This process create an opportunity that Au NPs are easily encapsulated into the MgO support, which generates a unique embedded structure that makes the Au nanoparticles firmly anchor onto the MgO support surface. Here, besides the arc-discharge breakdown, the repeated evolution of abundant oxygen gas of solution in high temperature and quenched environment also bring about the porous structure in MgO support.

With the time increase, the arc discharge become more intense and the coating layer (including MgO and Au species) quickly grow in thickness, which also cause the improved voltage. When the thickness of coating layer reaches a certain level, the film would not be broken down by high voltage due to its high resistance and the arc-discharge would gradually disappears, which indicate the end of PEO process.

The instruction of working mode in PEO

In generally, the input alternating current would go through two processes to arrive the electrode in PEO process. The detailed route is illustrated as Scheme S1: alternating current to rectifier to chopper and finally arrived to electrode.

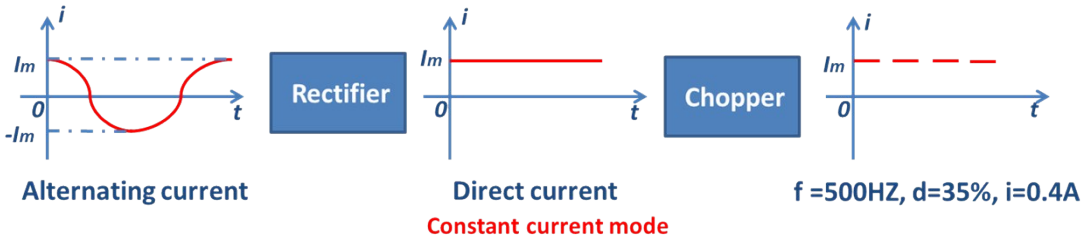

Scheme S1. Schematic process of the input current route in PEO process.

First, the alternating current would be converted into direct current by a rectifier in the PEO facility. Next, this generated direct current could be loaded into a chopper in three different modes: **constant current, constant voltage and constant power.** In our experiment, the **constant current mode** was selected, i=0.4A (This is the reason why we called this mode as a ' galvanostatic mode ' based on the International principle). After that, the chopper would modulate the input **constant current** by the frequency and duty cycle (f=500 Hz, d=35 %) and finally output to the electrode. In fact, the output current is a pulse current (not a constant) due to the frequency and duty cycle parameters.

The catalytic activity of Ru/MgO and Pd/MgO catalyst

(1) **Ru/MgO catalyst:** In this experiment, the hydrolysis of sodium borohydride was selected to evaluate the Ru/MgO catalytic activity. Firstly, 0.15 g sodium borohydride was solved in 50 mL alkaline H_2O solution ($C_{NaOH}=10^{-2}$M, pH=12) in a round flask as the reaction solution. Before catalytic reaction, the flask was placed in a water path to maintain the temperature at 30 ^oC. Next, Ru/MgO catalyst sample was putted in the flask and the hydrolysis reaction was trigger under magnetic stirring at 1500 r/min. The generated H_2 was measured by water displacement method as described in literature that H_2 push out water into a conical flask, which is placed on the electronic balance that is connected to a notebook computer. Here, the volume value of producing H_2 is equal to the water weight.

Catalytic activity: The catalytic activity of Ru/MgO for the hydrolysis of sodium borohydride was expressed by the hydrogen generation rate (***HGR*$_{H2}$**), which was calculated as follow:

$$HGR_{H2}=V_{total}/(t_{reaction}*m_{metal})$$

Where $\mathbf{V_{total}}$ is the total volume of generated H_2, $\mathbf{t_{reaction}}$ is the reaction time, and $\mathbf{m_{metal}}$ is the quality of Ru obtained by ICP measurement.

(2) **Pd/MgO catalyst:** the oxidation of silane was applied to measure the Pd/MgO catalytic activity. Catalytic reaction process is as follows. Simply, a 1mL Dimethyl phenyl silane, 500 μL H_2O were added to 20 mL acetone as the reaction solution. Then, the catalyst was immersed in mixture solution that was stirred at 1500 r/min under oxygen atmosphere. In the reaction process, sample was extracted from mixture every 1h and detected by GC (gas chromatography) using the ethylbenzene as internal standard. The chromatographic condition was set as below: chromatographic column HP-5, injector temperature 230 ^oC, distribution ratio of flow 10:1, injection volume 2 μL, FID detector temperature 280 ^oC; Temperature programming: 40 ^oC retain 0.5 min, temperature rise with 20 ^oC/min until arrive to 200 ^oC, retain 0.5 min.

Catalytic activity: The catalytic activity of Pd/MgO for oxidation of silane was expressed by the turn-over-number (TON), which was calculated as follow:

$$\mathbf{TON=n_{total\ product}/n_{metal}}$$

Where $\mathbf{n_{total\ product}}$ is total amount of reaction product, $\mathbf{n_{metal}}$ is the mole number of Pd.

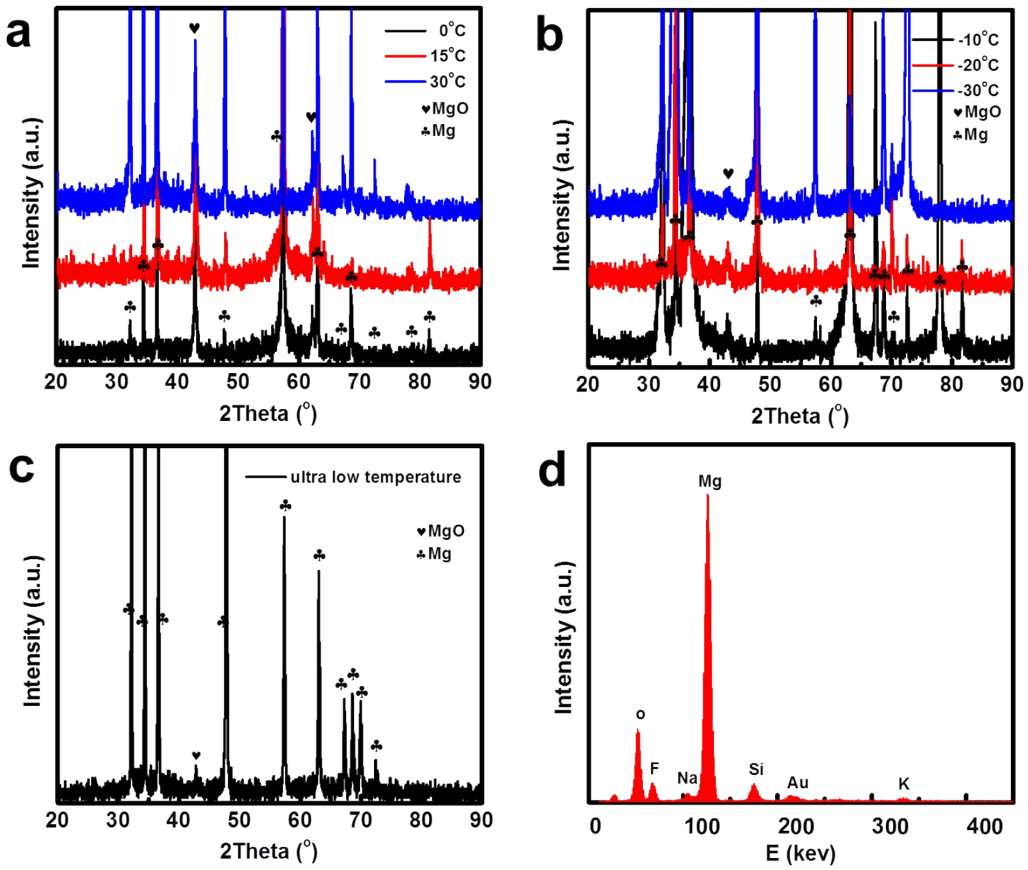

Fig. S1 XRD spectrum of Au/MgO catalyst prepared by PEO in different cooling conditions. (a) 0-30°C, (b) -10--30°C, (c) LN cooling. (d) EDS spectrogram of Au/MgO catalyst.

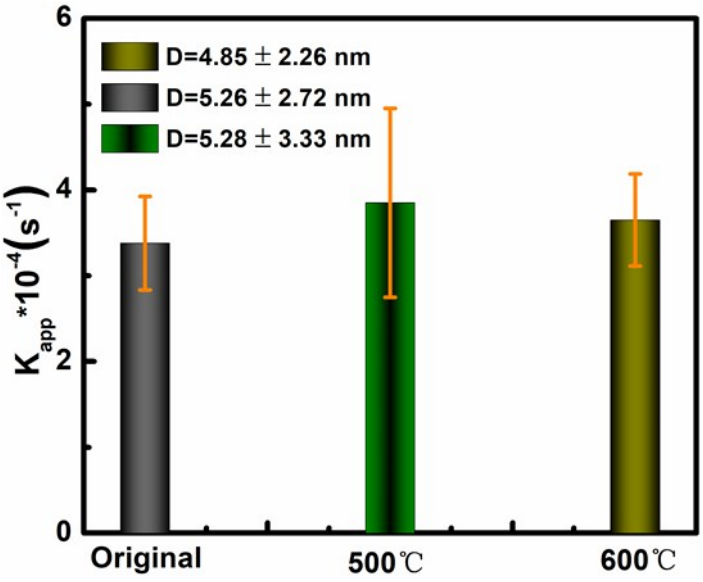

Fig. S2 The catalytic activity of Au/MgO catalyst treated by calcination at different temperature; the activity is corresponding to the sample PEO in Table S1.

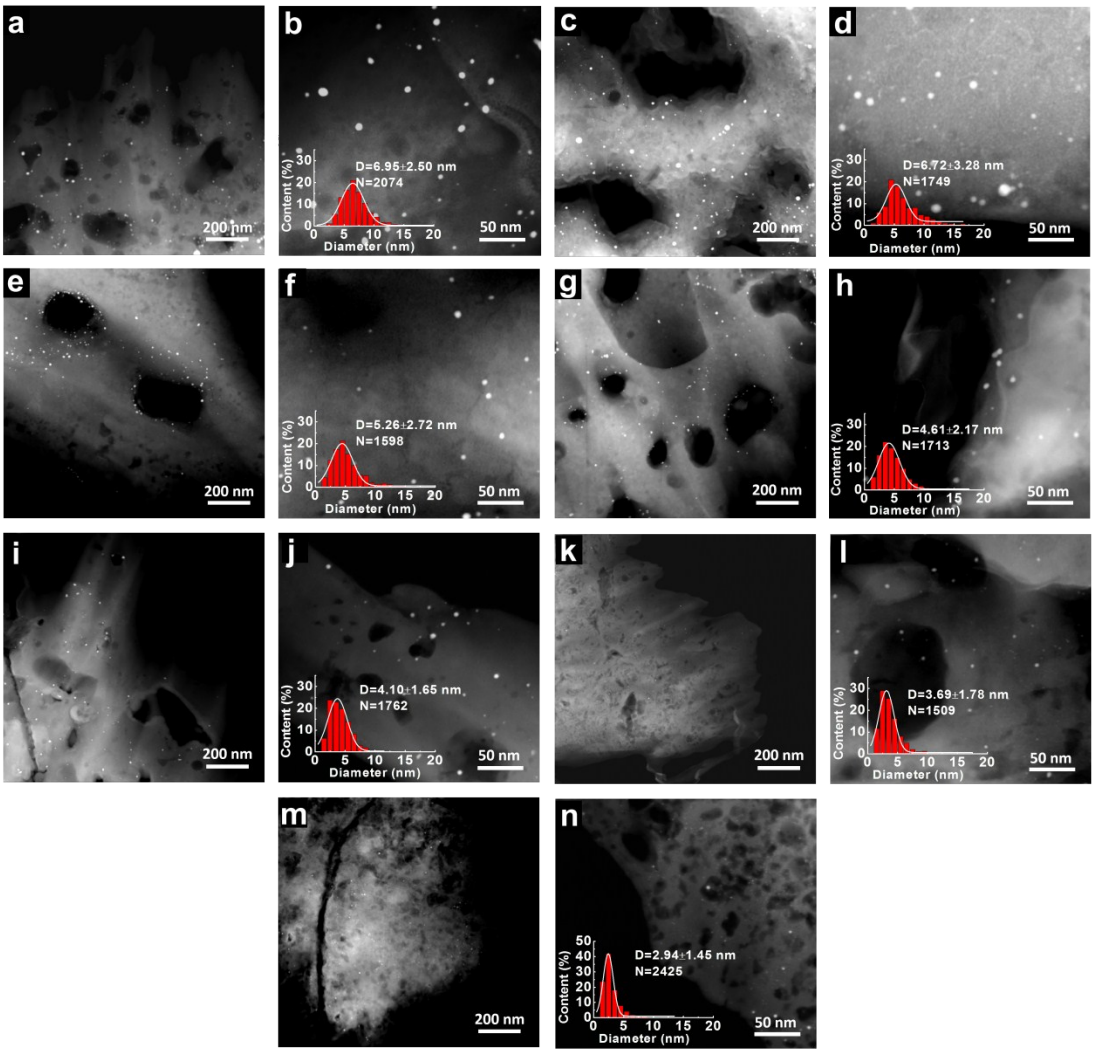

Fig. S3 HAADF-STEM images and magnification images of Au/MgO catalyst prepared by PEO in different cooling conditions. (a, b) 30 °C, (c, d) 15 °C, (e, f) 0°C, (g, h) -10 °C, (i, j) -20 °C, (k, l) -30 °C, (m, n) LN cooling and corresponding size distribution of Au NPs.

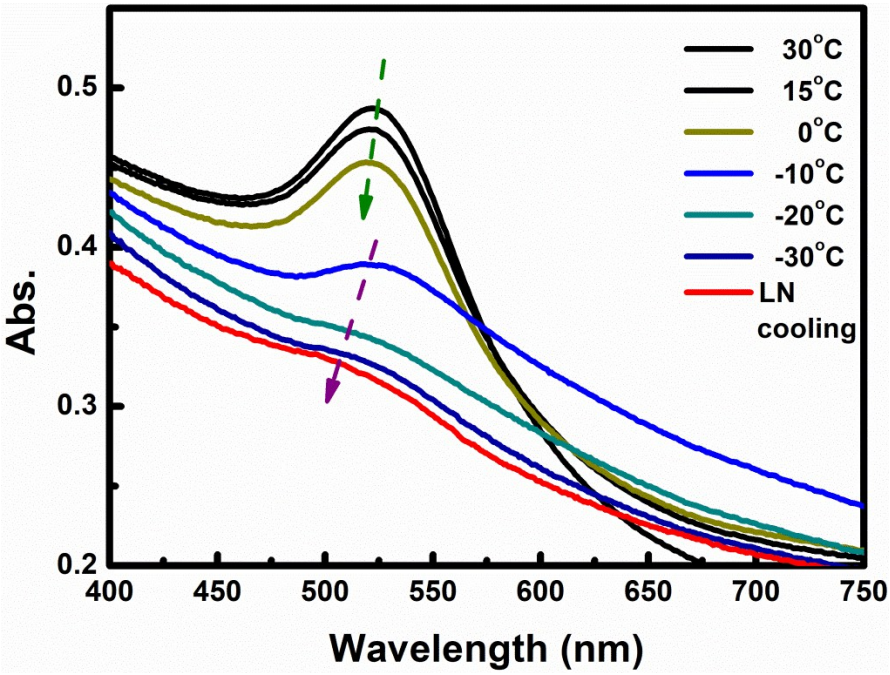

Fig. S4 UV-vis of Au/MgO prepared by PEO in different cooling conditions.

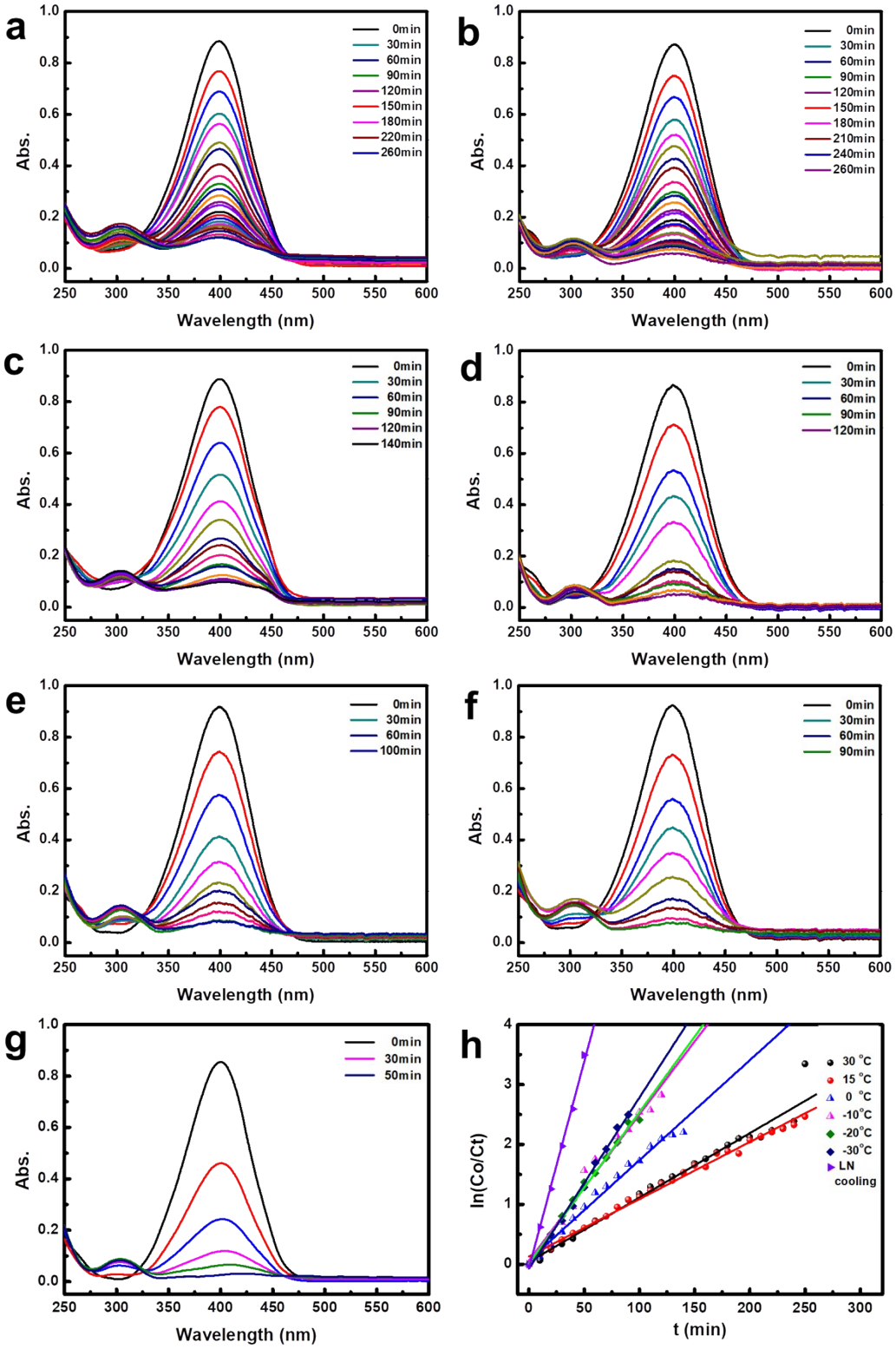

Fig. S5 UV-vis spectra evolution of the conversion of 4-NP into 4-AP using Au/MgO catalyst (the same content of Au) prepared by PEO in different cooling temperatures. (a) 30 °C, (b) 15 °C, (c) 0 °C, (d) -10 °C, (e) -20 °C, (f) -30 °C, (g) ULTPEO, (h) The plot of $\ln(C_o/C_t)$ *vs* reaction time for the disappearance at 400 nm.

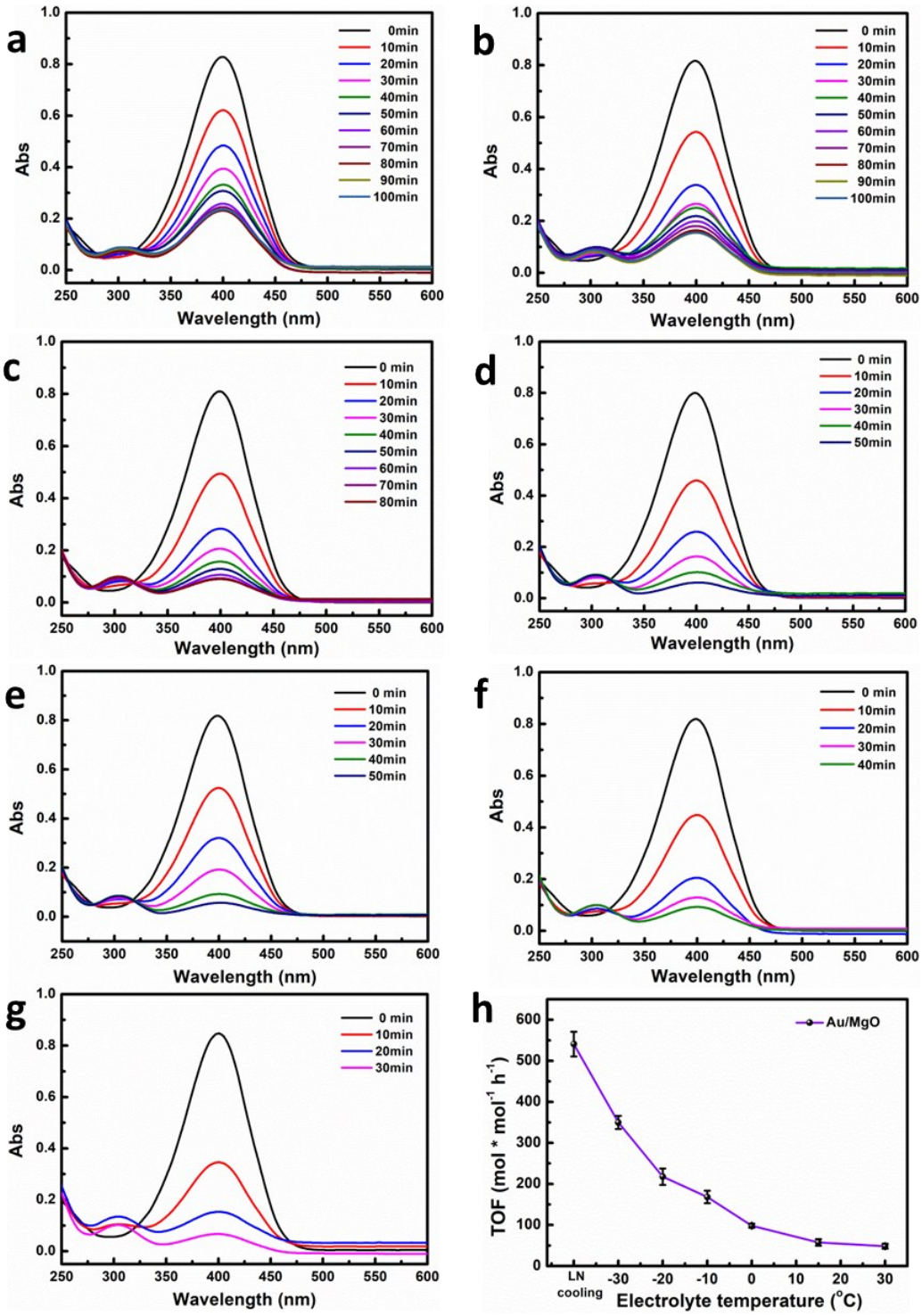

Fig. S6 UV-vis spectra evolution of the conversion of 4-NP into 4-AP using Au/MgO catalyst (using the same area of Mg substrate) prepared by PEO in different cooling temperatures. (a) 30 °C, (b) 15 °C, (c) 0 °C, (d) -10 °C, (e) -20 °C, (f) -30 °C, (g) ULTPEO, (h) The TOF value of the reaction using Au/MgO catalyst prepared in different cooling temperatures.

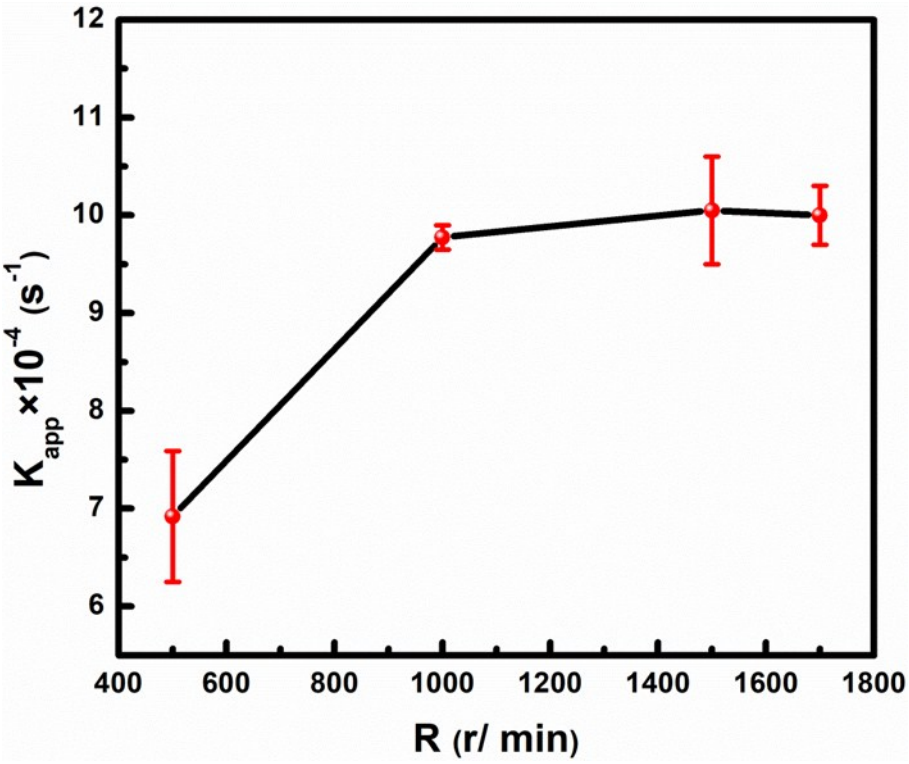

Fig. S7 The rate constant *vs* the stirring rate for the catalytic reaction using Au/MgO catalyst prepared in LN cooling.

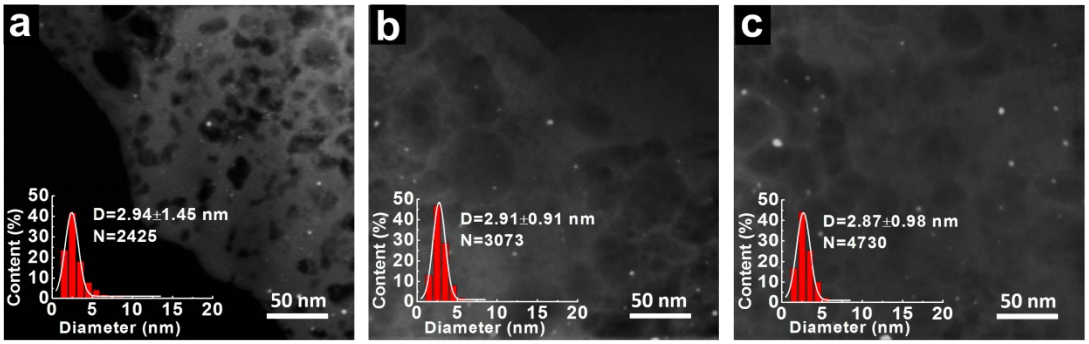

Fig. S8 HAADF-STEM images of Au/MgO catalyst prepared by ULTPEO at (a) unreacted condition, (b) 10 cycles, (c) 50 cycles and corresponding size distribution of Au NPs.

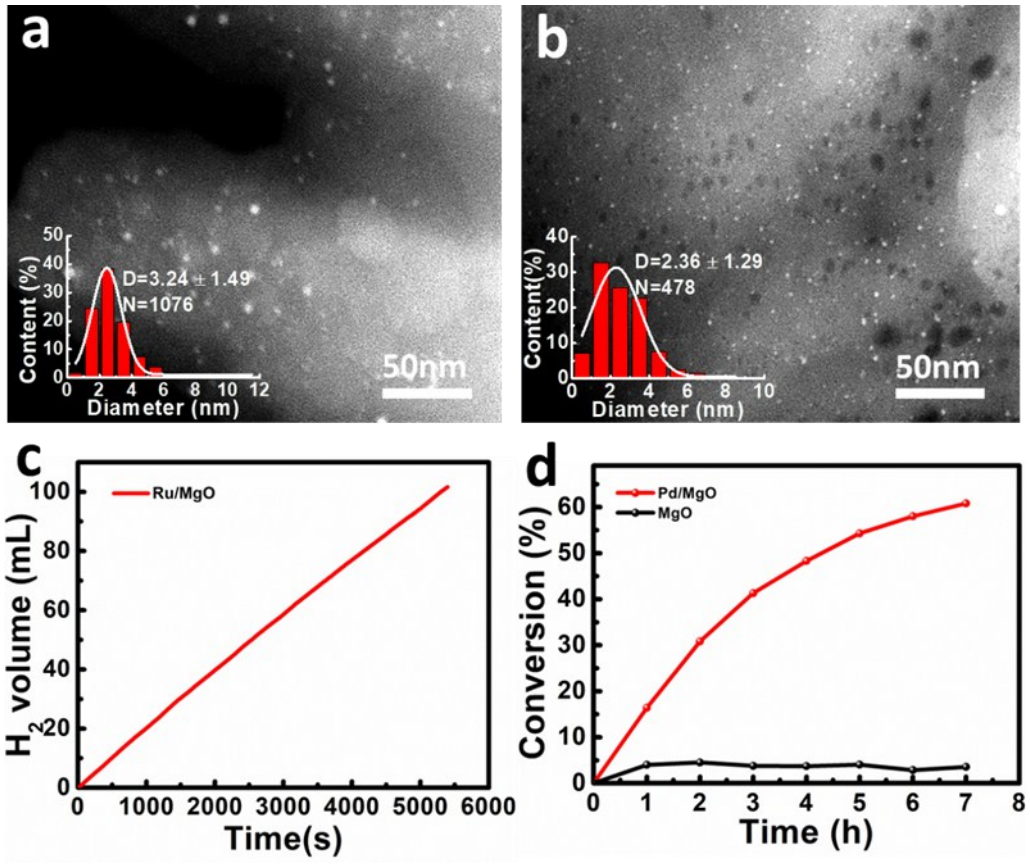

Fig. S9 HAADF-STEM images of the Ru/MgO and Pd/MgO catalyst prepared by PEO at 0 °C electrolyte. Experimental conditions: the content of Ru and Pd in used catalyst is 51 μg and 17.4 μg, respectively; HGR_{H2}=2.2*10^4 mL min^{-1} g^{-1}, TON silanol, 7h =24887.

Table S1. The size of the Au NPs in three catalysts by calcination treatment at different

temperature.

Sample[a]	Original (nm)	500℃ 2 h (nm)	600℃ 2h (nm)
PEO	**5.26±2.72**	**5.28±3.33**	**4.85±2.26**
DP	5.11±3.28	8.84±4.08	17.39±6.20
IM	4.94±1.09	9.71±4.73	12.26±4.97

[a] Experiment conditions: the Au/MgO sample was prepared by PEO at 0 °C electrolyte. The DP and IM sample were prepared according to the literature.[1,2]

Table S2. The TOF and TON value for the reaction of 4-nitrophenol using Au catalyst loaded various supports in literature.

Support catalyst	diameter (nm)	solution	lifetime (h)	TOF(b) (h^{-1})	TON (c) (lifetime)
Boehmite film@Au[3]			2	126	252
Polyaniline Nanofibers@Au[4]	10/2	water	0.5	19	9.5
graphene oxide/SiO2@Au[5]	5	water	-	210	-
nona-PEG-branched dendrimers@Au[6]	1.8	water	0.1	900	90
COF@Au[7]	5	water	1.3	8.06	10.5
CeO_2@Au[8]	8	water	0.67	240	160.8
Silica nanotube @Au[9]	3	water	-	0.7	-
PNIPAM-miclles@Au[10]	3.3	water	1.6	15.5	24.8
TWEEN/GO@Au[11]	6	water	-	6.9	-
hollow silica @Au[12]	2.8-4.5	water	0.17	560	95.2
D@GOCOOH@$(PAH/PAA)_6$@AuNPs[13]	5-8	water	1.33	111.6	148.4
Au@Fe3O4 Yolk-Shell [14]	2.5	water	0.83	300	249
Fe_3O_4@SiO_2@P(4VP-DVB)@Au[15]	5	water+ alcohol	2.5	4370	10925
TP-GS@Au[16]	1.5	water	0.5	3.62	1.81
DHBC@Au[17]	10	water		800	
PVP@Au[18]		water	4	0.8	3.2
PEI/PVP@Au[19]	11.8	water	1.8	0.63	1.13
CPSQ/Au[20]	2-5	water	3	96.6	289.8
PANI Nanofiber@Au[21]	2	water	0.5	68	34
PDDA/NCC@Au[22]	3	water		212	

methyl-imidazolium ionicpolymer[23]	1.8-2.8	water		22.2	
petide@Au[24]	2.3	water		3.75	
$(PLA/AuNP\text{-}HSA)_3$ NTs[25]	1	water	2.7	0.2	5.4
CNT/PHBP@Au[26]	6.7	water	4	8.75	35
TiO_2@Au[27]	10	water	1.25	40	50
CeO_2@Au[28]	5	water	0.33	2.5	0.83
Chitosan/Fe_3O_4@Au[29]		water	1.83	709	1300
Fe_3O_4@P(EGDMA-co-MAA)@Au[30]	1.18	water	0.1	1029	102.9
MgO@Au[31]	5-7	Water	0.92	1153	1057
Fe_3O_4/TiO_2@Au[32]	5	water	0.83	142	118
Au/MgO (30 °C)[a]	**6.95**	**water**	**8.75**	**48.5**	**426.8**
Au/MgO (15 °C)[b]	**6.6**	**water**	**8.75**	**57.4**	**528.1**
Au/MgO (0 °C)[c]	**5.6**	**water**	**8.75**	**98.4**	**875.8**
Au/MgO (-10 °C)[d]	**4.6**	**water**	**8.75**	**168.2**	**1513.8**
Au/MgO (-20 °C)[e]	**4.2**	**water**	**8.75**	**217.7**	**2363.8**
Au/MgO (-30 °C)[f]	**3.7**	**water**	**8.75**	**382**	**3285.2**
Au/MgO (LN cooling)[g]	**2.9**	**water**	**8.75**	**540.7**	**4731.1**
Au/MgO(LN cooling)[h](5 times)	**2.9**	**water**	**8.75**	**1378**	**12126**
Au/MgO(LN cooling)[i] (10 times)	**2.9**	**water**	**8.75**	**1643.4**	**14380**

[b] The TOF value was calculated based on the per gold atom exposed to the surface of Au nanoparticles.[58,59] The percentage of surface atoms to total atoms in Au nanoparticle is about 0.9/d (d is nanoparticle diameter in nm) according the literature.[60] [c] The TON value in this table is calculated as TOF*time h, where h referred to the whole lifetime of catalyst. Note: the content of Au in our catalysts are (a) 16.75, (b) 13.6, (c) 9.45, (d) 6.63, (e) 4.6, (f) 3.23, (g) 2.16 μg according to the different cooling conditions. The last two Au/MgO samples (h) and (i) were used in the reduction of 4-nitrophenol that the concentration of the substrate respectively increased 5 and 10 times compared to the previous reaction.

Table S3. The activation energy for the reaction of 4-nitrophenol using various Au catalysts prepared as reported by literature.

Catalyst	**Support**	**Activation energy (kJ/mol)**	**Refernece**
Au/PMMA	PMMA	38	[33]
Au/polyelectrolyte brushes	polyelectrolyte brushes	43	[34]
Au/ion-exchange resin	ion-exchange resin	31	[35]
Au/PDDA/NCC	nanocrystalline cellulose	69.2	[36]

CTAB-stabilized Au rods	----	38	[37]
Magnetically recoverable AuNPs	Fe_3O_4	52	[38]
Au nanoboxes	----	44	[39]
hollow Au nanoboxes	----	55	[39]
Au nanocages	----	28	[39]
HNTs/Au NCs	Aminosilane modified halloysite nanotubes	27	[40]
Au/calcium-alginate	calcium-alginate	21	[41]
(DMF)-stabilized Au NCs	----	31	[42]
Au/ mung bean starch	mung bean starch	47	[43]
Au/oxidized mesoporous carbon	Oxidized mesoporous carbon	86.8	[44]
Au/ black phosphorus	black phosphorus	17.53	[45]
Au/ hybrid microgels	hybrid microgels	36	[46]
Au nanorattles	----	29	[47]
Au@Ag nanocubes	----	38	[47]
Au nanosphere	----	41	[47]
silica-coatedgold nanorods	----	54	[48]
Au/MgO	**MgO**	**14.4**	**Our work**

Table S4. The comparison of recyclability for catalysts prepared by various methods in the reaction of 4-nitrophenol (4-NP).[d]

Nanoparticles	Support	Method	Recyclability (n)	Reference
Au	Hollow mesoporous CeO_2	colloidal deposition	8	[49]
Au	MWCNT-B	chemical grafting deposition	2	[50]

Au	No	in situ reduction technique	1	[51]
Ag	graphene oxide	solid-state chemical reaction method	7	[52]
Pt	micellar nanocomposites	chemical reaction method	5	[53]
Cu	graphite oxide	wetness impregnation technique	9	[54]
Ni	Mn_2O_3	co-reduction method	1	[55]
Ni	silica nanotubes	thermal decomposition and reduction	9	[56]
Ag-Co	RGO	gradual reduction method	3	[57]
Au	**Porous MgO**	**ULTPEO**	**>35**	**Our work**

[d] Contrast conditions: the conversion of 4-NP to 4-AP is decreased from 100% to 75% in catalytic reaction process.

References

1 M. Boronat, A. Corma, F. Illas, J. Radilla, T. Rodenas and M. J. Sabater, J. Catal., 2011, 1, 50-58.

2 V. R. Choudhary and D. K. Dumbre, Catal. Commun., 2009, 13, 1738-1742.

3 D. Jana, A. Dandapat and G. De, Langmuir, 2010, 26, 12177-12184.

4 J. Han, L. Li and R. Guo, Macromolecules, 2010, 43, 10636-10644.

5 C. Zhu, L. Han, P. Hu and S. Dong, Nanoscale, 2012, 4, 1641-1646.

6 L. Na, M. Echeverria, S. Moya, J. Ruiz and D. Astruc, Inorg. Chem. 2014, 53, 6954-6961.

7 P. Pachfule, S. Kandambeth, D. Dıàz Dıàz and Rahul Banerj, Chem. Commun., 2014, 50, 3169-3172.

8 B. Liu, S. Yun, Q. Wang, W. Hu, P. Jing, Y. Liu, W. Jia, Y. Liu, L. Liu, and J. Zhang, Chem. Commun., 2013, 49, 3757-3759.

9 Z. Zhang, C. Shao, P. Zou, P. Zhang, M. Zhang, M. Mu, Z. Guo, X. Li, C. Wang and Y. Liu, Chem. Commun., 2011, 47, 3906-3908.

10 Y. Wang, G. Wei, W. Zhang, X. Jiang, P. Zheng, L. Shi and A. Dong, J. Mol. Catal. A-Chem., 2007, 266, 233-238.

11 W. Lu, R. Ning, X. Qin, Y. Zhang, G. Chang, S. Liu, Y. Luo and X. Sun, J. Hazard. Mater., 2011, 197, 320-326.

12 S. H. Wu, C.T. Tseng, Y.S. Lin, C.H. Lin, Y. Hung and C.Y. Mou, J. Mater. Chem., 2011, 21, 789-794.

13 X. N. Zhao, T. F. Jiao, X. L. Ma, H. Huang, J. Hu, Y. Qu, J. X. Zhou, L. X. Zhang, Q. M. Peng, J. Taiwan. Inst. Chem. E., 2017, 80, 614-623.

14 F. H. Lin, R. A. Doong, J. Phys. Chem. C., 2017, 121, 7844-7853.

15 W. Guo, Q. Wang, Y. Luan, G. Wang, W. Dong and J. Yu, Chem. – Asian J., 2015, 10, 701-708.

16 R. Ren, S. W. Li, J. Li, J. X. Ma, H. Z. Liu and J. T. Ma, Catal. Sci. Technol., 2015, 5,

2149-2156.
17 E. Y. Seo, J. Kim, Y. J. Hong, Y. S. Kim, D. Lee and B. S. Kim, J. Phys. Chem. C., 2013, 117, 11686-11693.
18 C. Xiao, S. Chen, L. Zhang, S. Zhou, W. Wu, Chem. Commun., 2012, 48, 11751-11753.
19 X. Feng, H. Ma, S. Xiao, M. Shen, R. Guo, X. Cao, X. Shi, J. Mater. Chem., 2011, 21, 4493-4501.
20 F. Dong, W. Guo, S.K. Park, C.S. Ha, Chem. Commun., 2012, 48, 1108-1110.
21 J. Han, L. Li, R. Guo, Macromolecules, 2010, 43, 10636-10644.
22 E. Lam, S. Hrapovic, E. Majid, J.H. Chong, J.H.T. Luong, Nanoscale, 2012, 4, 997-1002.
23 I. Biondi, G. Laurenczy, P.J. Dyson, Inorg. Chem., 2011, 50, 8038-8045.
24 Y. Li, Z. Tang, P.N. Prasad, M.R. Knecht, M.T. Swihart, Nanoscale, 2014, 6, 3165-3167.
25 S. Goto, Y. Amano, M. Akiyama, C. Bottcher, T. Komatsu, Langmuir, 2013, 29, 14293-14300.
26 H. Li, J.K. Jo, L. Zhang, C.S. Ha, H. Suh, I. Kim, Adv. Funct. Mater., 2010, 20, 3864-3873.
27 A.A. Ismail, A. Hakki, D.W. Bahnemann, J. Mol. Catal. A: Chem., 2012,358, 145-151.
28 C.M. Fan, L.F. Zhang, S.S. Wang, D.H. Wang, L.Q. Lu, A.W. Xu, Nanoscale, 2012, 4, 6835-6840.
29 Y. C. Chang, D.H. Chen, J. Hazard. Mater., 2009, 165, 664-669.
30 H. Woo, K.H. Park, Catal. Commun., 2014, 46, 133-137.
31 K. Layek, R. Chakravarti, M.L. Kantam, H. Maheswaran and A. Vinu, Green Chem., 2012, 14, 3164-3174
32 W. T. Hu, B.C. Liu, Q. Wang, Y. Liu, Y.X. Liu, P. Jing, S.L. Yu, L.X. Liu, J. Zhang, Chem. Commun., 2013, 49, 7596-7598.
33 K. Kuroda, T. Ishida, M.Haruta, J. Mol. Catal. A: Chem., 2009, 298, 7-11.
34 M. Schrinner, F. Polzer, Y. Mei, Y. Lu, B. Haupt, M. Ballauff, A. Göldel, M. Drechsler, J. Preussner and U. Glatzel, Macromol. Chem. Phys., 2007, 208, 1542-1547.
35 S. Panigrahi, S. Basu, S. Praharaj, S. Pande, S. Jana, A. Pal, S.K. Ghosh, T. Pal, J. Phys. Chem. C, 2007, 111, 4596-4605.
36 E. Lam, S. Hrapovic, E. Majid, J. H. Chong and J. H. T. Luong, Nanoscale, 2012, 4, 997-1002.
37 Y. Khalavka, J. Becker and C. S€onnichsen, J. Am. Chem. Soc., 2009, 131, 1871-1875.
38 Y. C. Chang and D. H. Chen, J. Hazard. Mater., 2009, 165, 664-669.
39 J. Zeng, Q. Zhang, J. Chen and Y. Xia, Nano Lett., 2010, 10, 30-35.
40 S. Das and S. Jana, Dalton Trans., 2015, 44, 8906-8916.
41 S. Saha, A. Pal, S. Kundu, S. Basu and T. Pal, Langmuir, 2010, 26, 2885-2893.
42 H. Yamamoto, H. Yano, H. Kouchi, Y. Obora, R. Arakawa and H. Kawasaki, Nanoscale, 2012, 4, 4148-4154.

43 S. Chairam, W. Konkamdee and R. Parakhun, J. Saudi. Chem. Soc, 2017, 21, 656-663.
44 P. C. Guo, L. Tang, J. Tang, G. M. Zeng, B. B. Huang, H. R. Dong, Y. Zhang, Y. Y. Zhou, Y. C. Deng, L. L. Ma and S. R. Tan, J. Colloid Interface Sci. 2016, 469, 78-85.
45 J. Peng, Y. Q. Lai, Y. Y. Chen, J. Xu, L. P. Sun and J. Weng, small, 2017, 13, 1-11.
46 A. Pich, A. Karak, Y. Lu, A. K. Ghosh and H. J. P. Adler, J Nanosci Nanotechno, 2016, 6, 3763-3769.
47 S. Prem, R. Shounak and J. Amit, J. Phys. Chem. C, 2017, 121, 22914-22925.
48 M. Son, J. Lee and D. J. Jang, J. Mol. Catal. A: Chem., 2014, 385, 38-45.
49 B. Liu, S. Yu, Q. Wang, W. Hu, P. Jing, Y. Liu, W. Jia, Y. Liu, L. Liu, J. Zhang, Chem. Commun., 2013, 49, 3757-3759.
50 C. Fernandes, C. Pereira, A. Guedes, S. L. H. Rebelo and C. Freire, Appl. Catal. A-Gen., 2014, 486, 150-158.
51 M. H. Rashid and T. K. Mandal, Adv. Funct. Mater., 2008, 18, 2261-2271.
52 Y. Z. Li, Y. L. Cao, J. Xie, D. Z. Jia, H. Y. Qin and Z. T. Liang, Catal. Commun., 2015, 58, 21-25.
53 G. Q. Gao, L. Lin, C. M. Fan, Q. Zhu, R. X. Wang and A. W. Xu, J. Mater. Chem. A, 2013, 1, 12206-12212.
54 M.V. Morales, M. Roch, C. Freire, E. A. Nieto, E. Gallegos-Suarez, I. Rodríguez-Ramos, A. Guerrero-Ruiz Morales, Carbon, 2017, 111, 150-161.
55 P. K. Deka, P. Sarmah, R. C. Deka and P. Bharali, ChemistrySelect, 2016, 1, 4726-4735.
56 S. H. Zhang, S. L. Gai, F. He, S. J. Ding, L. Li and P. P. Yang, Nanoscale, 2014, 6, 11181-11188.
57 R. Krishna, D. M. Fernandes, C. Dias, J. Ventura, E. V. Ramana, C. Freire, E. Titus, Int. J. Hydrog. Energy, 2015, 40, 4996-5005.
58 W. J. Li, A. Q. Wang, X. F. Yang, Y. Q. Huang and T. Zhang, Chem. Commun., 2012, 48, 9183-9185.
59 D. V. Jawale, Edmond Gravel, Valerie Geertsen, H. Y. Li, Nimesh Shah, Rahul Kumar, Jubi John, Irishi N.N. Namboothiri and Eric Doris, Tetrahedron , 2014, 70, 6140-6145.
60 M. Boudart, G. Djéga-Mariadassou in Kinetics of Heterogeneous Catalytic Reactions, Princeton University Press, Princeton, N. J., 1984, pp 26.